Pressure effect on the multicycle activity of natural carbonates and a Ca/Zr composite for energy storage of Concentrated Solar Power

*Beatriz Sarrion[1], Pedro E. Sanchez-Jimenez[1], Antonio Perejon[1,2], Luis A. Perez-Maqueda [1], Jose Manuel Valverde [3]**

[1]Instituto de Ciencia de Materiales de Sevilla, C.S.I.C.-Universidad de Sevilla, C. Américo Vespucio nº49, 41092 Sevilla, Spain.

[2]Facultad de Química, Universidad de Sevilla, Avenida Reina Mercedes s/n, 41012 Sevilla, Spain.

[3]Facultad de Física, Universidad de Sevilla, Avenida Reina Mercedes s/n, 41012 Sevilla, Spain.

*Prof. J.M. Valverde

Facultad de Física

Universidad de Sevilla

Avenida Reina Mercedes s/n, 41012 Sevilla (Spain)

Tel +34 954550960 Fax +34 954239434

E-mail: jmillan@us.es

KEYWORDS: Concentrated Solar Power, limestone, dolomite, $ZrO_2/CaCO_3$ composite, Calcium-Looping, energy storage.

ABSTRACT

This work is focused on the use of the Calcium-Looping process (CaL) in Concentrated Solar Power (CSP) plants for Thermochemical Energy Storage (TCES). Cheap, abundant and non-toxic natural carbonate minerals, such as limestone and dolomite, can be employed in this application to store energy through the cyclic calcination/carbonation of $CaCO_3$. In a recent work, a closed CO_2 cycle has been proposed for an efficient CaL-CSP integration in which the CO_2 in excess effluent from the carbonator is used to generate electricity by means of a gas turbine. Process simulations show that the thermoelectric efficiency is enhanced as the carbonator pressure and temperature are increased provided that the multicycle CaO conversion is not affected. On the other hand the use of just one reactor for both calcination and carbonation has been suggested to reduce capital cost. However, the experimental results shown in the present work indicate that sintering is notably enhanced as the pressure in the reactor is increased. Such adverse effect is mitigated for a $ZrO_2/CaCO_3$composite with a low Zr content as compared to natural carbonates. These results are relevant to process simulations for better assessing the global efficiency of the CaL-CSP integration.

INTRODUCTION

Concentrated Solar Power (CSP) is one of the main renewable energy technologies to be developed as it allows large scale electricity generation and relatively low-cost energy storage in the form of heat. Nowadays, there are a number of commercial CSP plants worldwide wherein molten salts are used for thermal energy storage (TES) as sensible heat [1-4]. However, there is a need of cheaper massive energy storage technologies to gain competitiveness against fossil fuel power plants [5-8]. A potentially more advantageous technique to store CSP is Thermochemical Energy Storage (TCES), which is currently under research and development [9-10]. TCES basically consists of using heat from concentrated solar irradiation (reaching temperatures up to ~1000°C in CSP with tower technology) to drive an endothermic chemical reaction. When energy is needed, the separately stored reaction byproducts are brought together to carry out the reverse exothermic reaction. Main advantages of TCES systems compared to TES is the higher storage energy density potentially attainable as well as the possibility of storing energy in the long term without significant losses [9, 11-12].

Among the diverse possibilities explored for TCES at large scale, one of the most promising technologies is based on the Calcium-Looping (CaL) process, which relies on the multicycle $CaCO_3$ calcination/carbonation (Eq. (1)) [13-14]. This application was proposed in the late 1970s [15-17] but has gained renewed interest only in recent years [9, 18-20]. The CaL process offers a great potential for large scale energy storage as cheap, non-toxic and abundant materials such as limestone and dolomite can be employed [18]. Moreover, the storage energy density of the system (~3.2 GJ/m^3) is notably higher than the energy density of molten salts currently used in commercial plants (~0.8 GJ/m^3 [21]).

$$CaCO_{3(s)} \rightleftarrows CaO_{(s)} + CO_{2\,(g)} \qquad \Delta H_r^0 = 178\ kJ/mol \qquad (1)$$

The CaL process has been widely investigated in recent years albeit most investigations have been oriented towards the CaL application for capturing CO_2 in fossil fuel fired power plants, which has been successfully demonstrated at the pilot scale (1-2 MW_{th}) [22]. The CaL process for CO_2 capture is based on the carbonation of CaO at temperatures around 650°C. CaO particles are fluidized by the post-combustion gas at an absolute pressure of 1 bar with a low concentration of CO_2 (15 vol%). The carbonated particles are then transported into a second fluidized bed reactor (calciner) where calcination is carried out at temperatures above 900°C under high CO_2 concentration. CO_2 is recovered from the calciner to be compressed and stored or employed for other uses. After calcination, the regenerated CaO particles are recirculated into the carbonator reactor for their use in a new cycle. The present manuscript is focused on the use of the CaL process for TCES in CSP plants according to a recently proposed integration scheme [18] (Fig. 1).

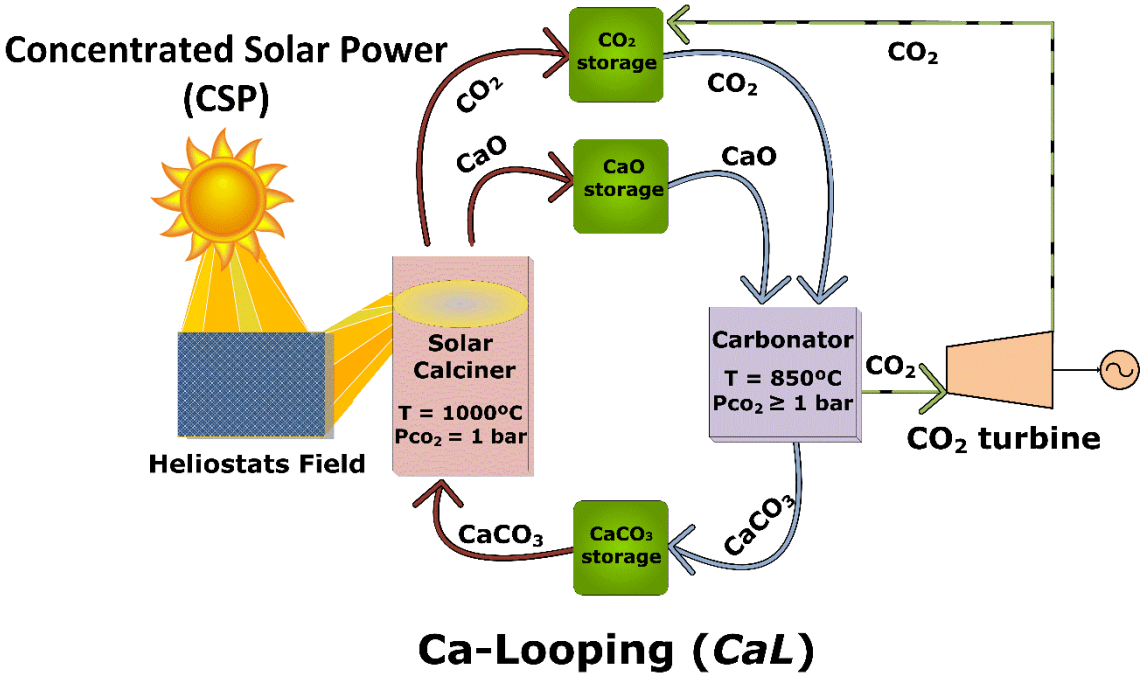

Fig. 1. Flow diagram of the Calcium-Looping thermochemical energy storage system for Concentrated Solar Power plants. The indicated calcination/carbonation conditions are those employed in the present work. A detailed description is found in [18].

The CaL-CSP integration essentially consists of a CO_2 turbine to generate power, a solar calciner, a carbonator, and two reservoirs for both CaO and $CaCO_3$ storage and a CO_2 compression-storage system. The process starts with the calcination of $CaCO_3$ particles using concentrated solar energy to provide the heat needed for the endothermic decomposition reaction (Eq. 1). The reaction byproducts, CaO and CO_2, are stored separately and afterwards circulated to the carbonator for the exothermic carbonation reaction to release the heat used for electricity generation in a gas turbine through a closed CO_2 circuit. According to process simulations [18], maximum global efficiency is achieved at CaL conditions involving carbonation under high CO_2 pressure (~3 bar) and high temperature (>~850°C). These results are based on the assumption that the multicycle CaO activity is not affected by the reactor pressure. However, the effect of successive cycles of calcination and carbonation under high pressure on the CaO multicycle activity has not investigated yet to our knowledge.

A possible strategy to save capital cost and technical complexity is to use just one reactor both as calciner and carbonator [23]. Since both stages would be carried out in one-day cycles, this simplification could be feasible. Nevertheless, it is uncertain whether the activity of the CaO regenerated in each cycle will be affected in practice by relevant limiting mechanisms such as sintering, which could be significantly enhanced at high CO_2 pressure under high temperature. In our work, we address this issue by a thermogravimetric experimental study on the multicycle CaL performance, at conditions for CSP storage (Fig. 1). The study analyzes the behavior of natural carbonates (limestone and dolomite) and a $ZrO_2/CaCO_3$ composite subjected to CaL cycles in a home-made reactor where pressure is changed between 1 bar for calcination and 3 bars for carbonation.

EXPERIMENTAL

Materials

Two natural carbonates have been used in our study: natural limestone (99.3 wt% $CaCO_3$) and dolomite from Taljedi quarry in Seville (Spain). Table S1 (supporting information) shows the chemical composition as measured X-Ray Fluorescence (XRF). Moreover, a $ZrO_2/CaCO_3$ composite was prepared by mechanical milling of a 5 wt% ZrO_2 / 95 wt% natural limestone powder mixture in an Emax high energy ball mill (Retsch GmbH). The mixture was milled for 90 s at 1500 rpm using a stainless steel jar and 50 stainless steel balls 10 mm diameter. A sample to ball mass ratio of 1:20 was employed, which corresponds to a total sample mass of 10 g. An important advantage of mechanical milling over other synthetic routes is its simplicity and scalability, which must be necessary attributes for any synthetic Ca composite to be employed in the CaL process at industrially relevant conditions. Note also that the ZrO_2 relative content of the mixture is rather low, which would also facilitate the use of the composite in practical applications.

The raw samples were sieved after which Particle Size Distributions (PSD) were measured by means of laser diffractometry using a Mastersizer 2000 instrument. The samples were previously dispersed in 2-propanol as recommended for Ca-based granular media and sonicated for 10 min to loosen particle aggregates. As seen in Fig. S1, the sieved samples of limestone, dolomite and the $ZrO_2/CaCO_3$ composite show a similar PSD with most of the particles lying in the range between 100 and 400 μm. A 95.3%, 96.5% and 87.2% of the particles population is within this range for dolomite, limestone and the $ZrO_2/CaCO_3$ composite, respectively. This particle size range is appropriate to be employed in industrial applications where the reactors are usually operated in the circulating fluidized bed (CFB) regime. Operation under this regime ensures optimum transfer of heat and mass as opposed to bubbling or fixed beds where heat/mass transfer is hampered. As shown in previous works focused on the CaL application for CO_2 capture, Ca-based sorbents exhibit a similar multicycle performance in large-scale pilot plants (1-2 MW_{th}) to that measured by means of thermogravimetry analysis (TGA) [24]. The use of very small amounts of sample in TGA serves to reproduce the optimum heat and mass transfer conditions achieved in CFBs used in large scale applications. Since particles are placed on the measuring vessel practically forming a monolayer undesired effects due to CO_2 diffusion resistance across the bulk of the powder are avoided. On the other hand, since most of the particles are of size below 400 μm, carbonation hindrance by the resistance due to intraparticle pore diffusion is minimized [25].

Characterization methods

Thermogravimetry measurements were carried out using a homemade thermobalance specially assembled for this purpose and able to work up to 5 bars (Fig. 2). The system basically consists of a high sensitivity ($2x10^{-7}$g) CI Electronics balance and a reactor. The reactor is a mullite-lined furnace built from a non-porous mullite tube (able to hold 5 bars of pressure), which is connected and sealed with the balance by means of pressure o-rings and clamps. The mullite-lined furnace is placed inside a Watlow furnace (VC402A06A, 120V, 425W). The reactor is coupled to two thermocouples to accurately control and measure the temperature. One is placed just below the sample crucible to measure the sample temperature and the other one is placed nearby the heater to control the heating rate. The whole system was sealed by means of pressure o-rings. A flat ceramic crucible (0.157cm^3, ~1200°C) was used. The themobalance was accurately calibrated by means of a set of calibration weights ranging from 0 mg to 100 mg. The R-squared value of the linear fit was 0.99998 (Fig. S2 in supporting information). Temperature calibration was performed from the well-known decomposition reaction of hydrous calcium oxalate, which was heated at 10 $Kmin^{-1}$. The buoyancy effect was corrected using alumina as a standard material. The setup incorporates pressure control valves, a pressure gauge and over-pressure protection. Mass flow and pressure controllers were employed to carry out the tests under a continuous 100 cm^3min^{-1} CO_2 flow and at constant absolute pressure (either 1 or 3 bar). Cooling tubes were located above and below the reactor and two fans were used to stabilize the working temperature.

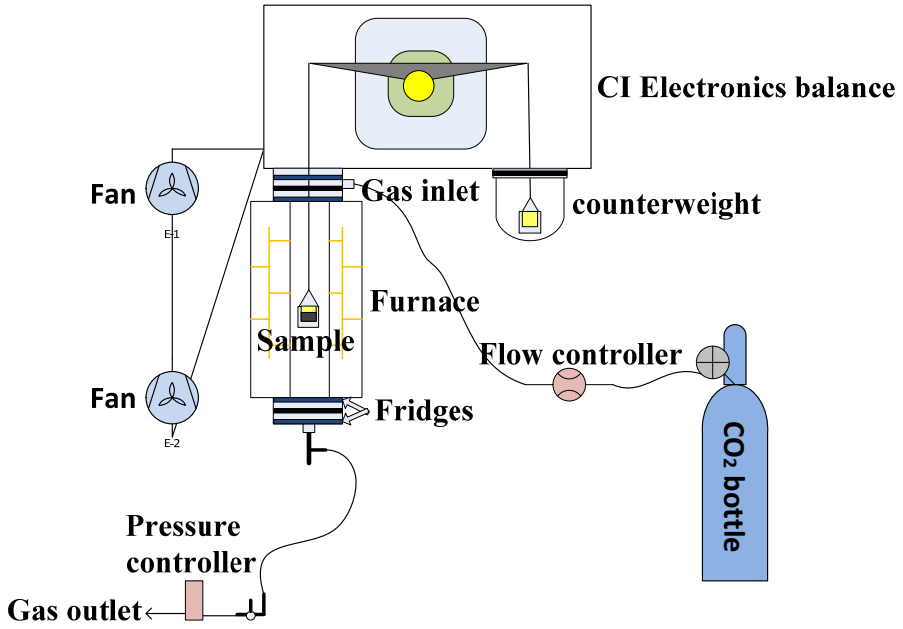

Fig. 2. Schematic diagram of the pressurized thermobalance system employed in the present work.

Both the carbonation and calcination stages were carried out under pure CO_2 (Fig. 1). For an operating pressure of 1 bar under CO_2, the maximum carbonation temperature is approximately 895°C according to thermodynamical equilibrium [26]. However, near the equilibrium temperature, the carbonation kinetics becomes very slow [27]. Thus, a carbonation temperature of 850°C, which yielded a fast-enough kinetics, was fixed for all the tests. On the other hand, the calcination temperature used was fixed to 1000 °C.

Multicycle calcination/ carbonation tests were started with a precalcination stage by increasing the temperature from room temperature to the calcination temperature (1000°C) at 10 °C/min under pure CO_2. For the tests carried out under absolute pressure of 1 bar, the temperature was decreased at 10°C/min to 850°C to carry out the carbonation stage, after which the temperature was again increased up to 1000°C for a new cycle.

Figure 3 shows the temperature and pressure time evolution for the tests in which carbonation was carried out at 3 bars. These experiments were also started by a precalcination stage from room temperature to the calcination temperature (1000°C) at 10°C/min. Then, the CO_2 pressure was increased up to 3 bars while the temperature was kept at 1000°C, after which the temperature was immediately decreased to 850°C at 10°C/min to carry out the carbonation stage under 3 bars. Following this protocol carbonation was started once the pressure was set at 3 bars. An alternative procedure, as the one followed by Butler et al. [28] by means of pressure swing, would have been to increase the pressure to 3 bars after the temperature is decreased to the target carbonation temperature (850°C) but, in that case, most of the carbonation would take place before reaching the target pressure of 3 bars, which does not adjust to practical conditions in the CaL application for energy storage. For these tests to have a practical utility, carbonation must be performed under high pressure to achieve a maximum thermoelectric efficiency according to simulations.

Once the carbonation stage had finished, the reactor absolute pressure was decreased to an absolute pressure of 1 bar, after which the temperature was increased to 1000°C for a new calcination stage. In order to avoid undesired effects due to CO_2 diffusion resistance across the bulk of the sample, small and similar masses (40 mg) were tested in all cases. Thus, optimum heat and mass transfer conditions as those existing in CFBs are mimicked in our setup [29].

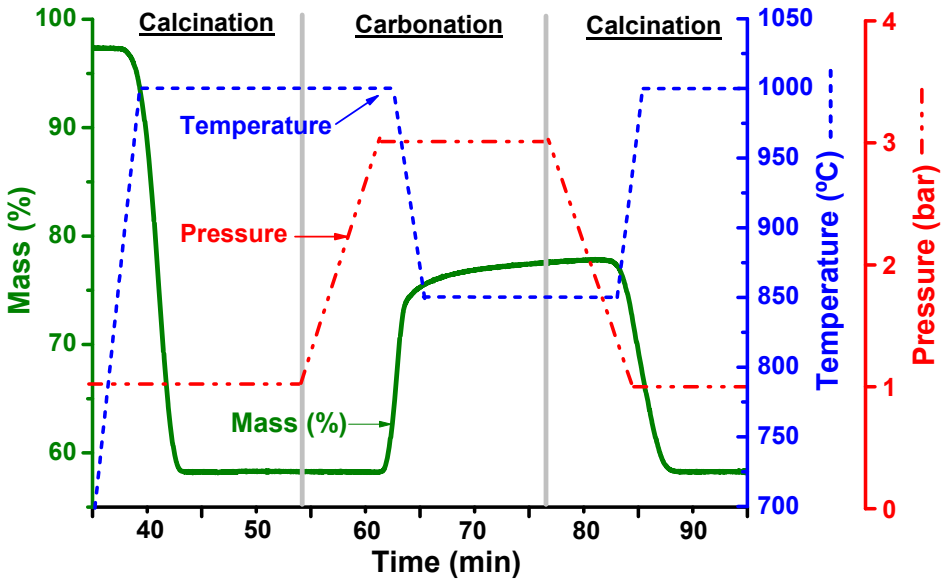

Fig. 3. Time evolution of sample mass (%), temperature (°C) and absolute pressure (bar) during a carbonation/calcination cycle under pure CO_2 for limestone. The carbonation stage was done in this example under 3 bars of pressure.

The morphology of the samples resulting after the CaL cycles was analyzed by Scanning Electron Microscopy (SEM) using a high-resolution HITACHI S4800 SEM-FEG microscope. Elemental composition analysis of the $ZrO_2/CaCO_3$ composite was carried out by means of focused ion beam scanning electron microscopy (FIB-SEM tomography) using a ZEISS AURIGA equipment. Full elemental composition analysis of the raw samples has been performed by X-ray microfluorescence using an Eagle III Micro XRF instrument (EDAX, New Jersey, USA) equipped with an X-ray anticathode 50 W rhodium tube and an energy dispersive X-ray detector and with a maximum operating potential of 40 keV and 1 mA. As may be seen in Table S1 (supporting information) the proportion of impurities present in the limestone and dolomite is (<0.6-0.7 wt%, which suggests that these trace elements do not have a significant effect on the measured multicycle performance.

RESULTS AND DISCUSSION

In order to objectively assess the multicycle activity performance of the materials employed in our work we have used the effective conversion X_{eff}, which is defined as the ratio of the mass of CaO converted in the carbonation reaction to the total sample mass before carbonation was started:

$$X_{effN} = \frac{m_{carbN} - m_N}{m_N} \cdot \frac{W_{CaO}}{W_{CO2}} \quad (2)$$

where m_N is the total mass of the sample in the Nth cycle just before carbonation and after calcination (including CaO and MgO in the case of dolomite, and CaO and ZrO_2 for the composite), m_{CarbN} is the sample mass once the carbonation stage is finished, and W_{CaO} (56 g/mol) and W_{CO2} (44 g/mol) are the molar masses of CaO and CO_2, respectively. The use of effective conversion, as opposed to CaO conversion, allows us to take into account the presence of inert oxides (MgO and ZrO_2 in this work) in the material, which have to be transported also in the practical application along with the active CaO.

Figure 4 shows a comparison of experimental data on the multicycle effective conversion measured for all samples at different carbonation pressures (1 and 3 bar). A relevant observation is that the increase of the carbonation pressure hinders the multicycle activity. Figure 5a shows a comparison of multicycle conversion data measured for the three materials at high pressure carbonation. The relative decrease of conversion with respect to carbonation under 1 bar is shown in Fig. 5b. As may be seen, the adverse effect of increasing the carbonation pressure becomes more noticeable in the case of limestone followed by dolomite. Comparatively higher values of conversion are measured for the $ZrO_2/CaCO_3$ composite under high pressure. Thus, the value of conversion under high pressure carbonation is X_{effN} = 0.22 for the composite compared to 0.15 for dolomite and just 0.07 for limestone. Interestingly, such notable improvement of performance under high pressure is obtained for the composite by adding just a 5% of mass of inert material (ZrO_2) to natural limestone.

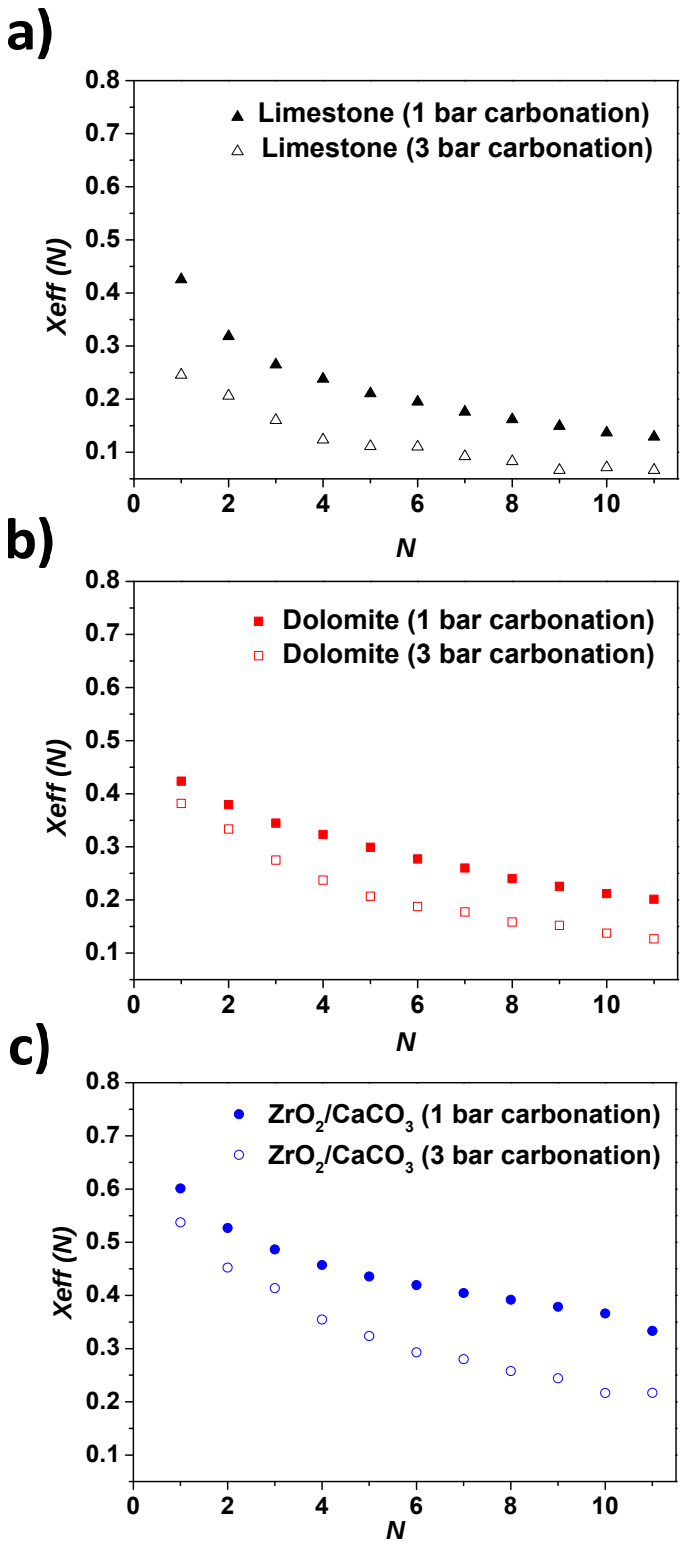

Fig. 4. Multicycle effective conversion data for natural limestone (a), dolomite (b) and $ZrO_2/CaCO_3$ composite (c) samples as a function of the number of carbonation/calcination cycles carried out under atmospheric and high pressure carbonation as indicated (calcination in CO_2 at 1000°C, carbonation under CO_2 at 850°C either at 1 or 3 bars of absolute pressure).

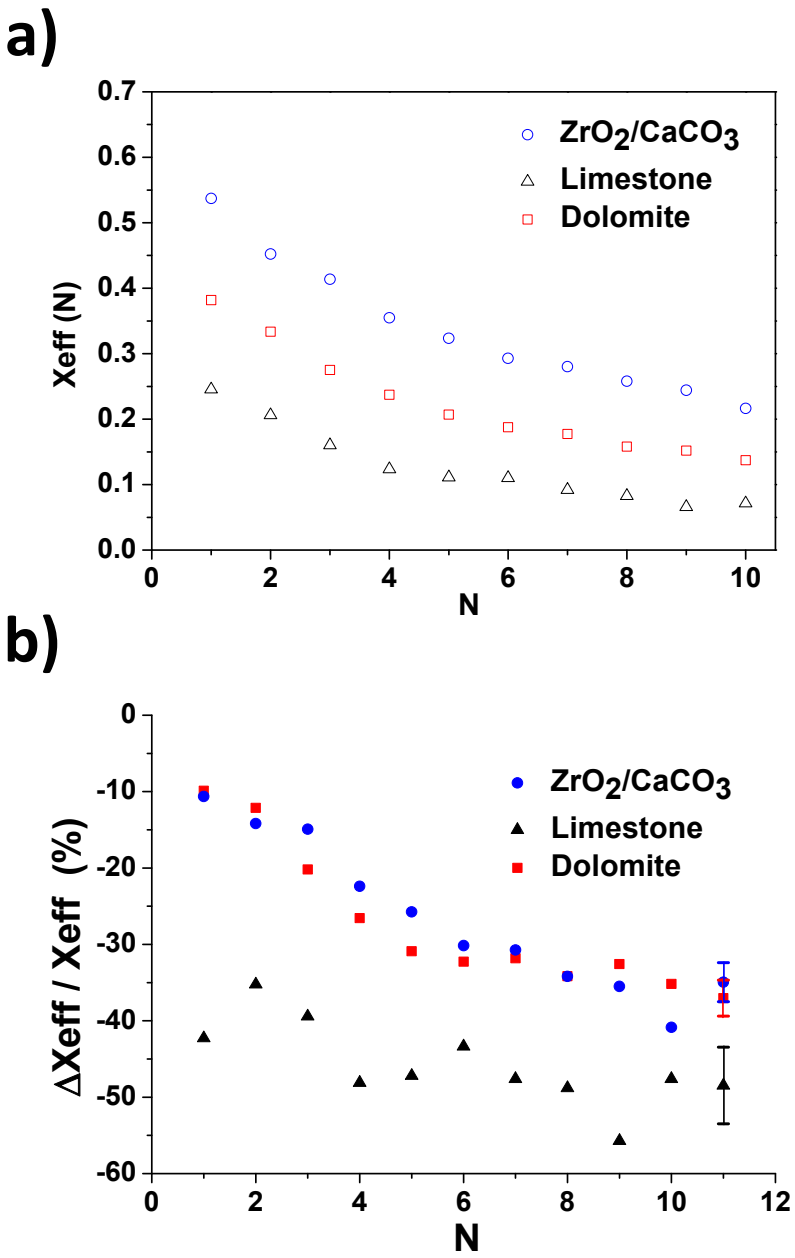

Fig. 5. a) Multicycle effective conversion data for natural limestone, dolomite and $ZrO_2/CaCO_3$ composite samples as a function of the number of carbonation/calcination cycles carried out under CaL–CSP storage conditions (calcination in CO_2 at 1000°C, carbonation in CO_2 under 3 bars of pressure at 850°C). b) Relative decrease of effective conversion [(Xeff under 3 bar – Xeff under 1 bar)/(Xeff under 1 bar)]x100 as a function of the number of carbonation/calcination cycles carried out under CaL–CSP storage conditions (calcination in CO_2 at 1000°C, carbonation under CO_2 at 850°C either at 1 or 3 bars as indicated). The error bars show the data uncertainty.

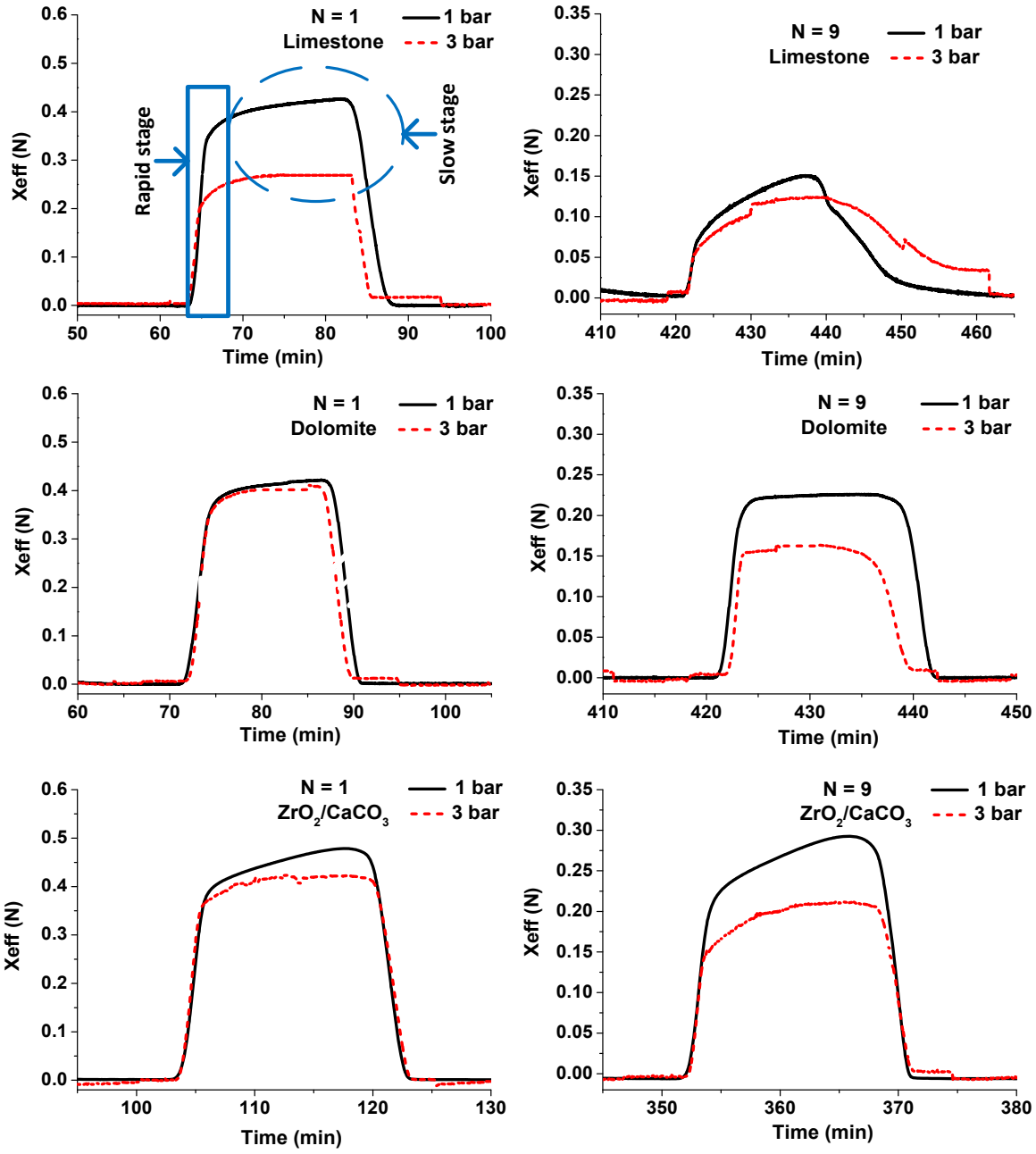

Fig. 6. Time evolution of CaO conversion during the 1st and 9th cycle for calcination/carbonation tests carried out under CaL–CSP storage conditions (calcination in CO_2 at 1000°C, carbonation under CO_2 at 850°C either at absolute pressure of 1 or 3 bar as indicated).

Figure 6 shows the time evolution of effective conversion measured for each sample during the carbonation and calcination stages of the 1st and 9th cycles. As well-known from previous studies, carbonation is seen to proceed through two well differentiated phases [30-31]. The first one is a rapid stage controlled by the reaction kinetics at the particles' surface [32] whereas the following slower phase is limited by the diffusion of CO_2 across the product layer of $CaCO_3$. Figure 6 shows that the fast reaction phase under high pressure (3 bar) is notably hindered already from the first cycle for CaO derived from limestone whereas such effect is not so significant for the

composite and dolomite samples. This suggests that CaO grains suffer a notable sintering during this high temperature/high pressure stage. The presence of inert MgO grains in the case of dolomite and ZrO_2 grains in the case of the composite would mitigate sintering of the CaO grains. The thermograms in the 9th cycle (Fig. 6) show that carbonation in the fast reaction controlled phase is severely hampered for limestone. Note also that the calcination rate is also hindered for the sample carbonated under high pressure as would be expected from the enhancement of $CaCO_3$ crystallinity that would be caused by the high pressure and high temperature carbonation [33]. As we have shown in previous studies there is a correlation between the degree of crystallinity of $CaCO_3$ and its calcination rate, the higher the crystallinity the slower the calcination [34]. Thus, after 11 cycles, calcination was incomplete in the residence time fixed despite the temperature used for calcination was quite high (1000ºC), which prevented us from further testing in successive cycles. Achieving calcination temperatures higher than 1000ºC from CSP is quite challenging technically, thus we stopped the tests after 11 cycles. Thus, the progressive slowdown of calcination as observed for limestone is also a relevant drawback for the CaL technology where both carbonation and calcination stages must proceed in short residence times [35]. In the case of dolomite and the $ZrO_2/CaCO_3$ composite the presence of impurities in the $CaCO_3$ crystal structure would allow decarbonation to proceed at a faster rate and this detrimental effect is not observed.

Figure 7 shows SEM pictures of cycled samples (CaL cycles ending in calcination). As may be seen, carbonation under 3 bars leads to a significant enhancement of CaO sintering and a reduction of porosity, especially in the case of limestone, which is consistent with the marked loss of activity derived from thermogravimetry (Fig. 4). Thus, the size of the CaO grains, which is on the order of 100 nm for the samples cycled at absolute pressure of 1 bar (Fig. 7a), is increased up to a few microns for the samples cycled under high pressure (Fig. 7b). On the other hand, the degree of CaO sintering is comparatively mitigated for dolomite and the $ZrO_2/CaCO_3$ composite. Thus, our study shows that CaO sintering would be notably promoted as the pressure in the reactor is increased. Note that the rather high calcination temperature (1000°C) is close to the CaO Tamman temperature ($T_t \simeq 1170$°C) [24]. At this temperature (about one-half of the melting temperature in K) the atoms in the solid acquire sufficient energy for their bulk mobility to become notable. Furthermore, the high CO_2 pressure would promote the aggregation of the nascent CaO crystals as enhanced CO_2 adsorption in the solid surfaces leads to an increase of interparticle attractive forces [24, 36]. Thus, the presence of CO_2 when the pressure is increased just before carbonation and in the initial stage of carbonation would enhance sintering of the CaO grains, which would hinder carbonation in the fast reaction stage as seen in Fig. 6 from the 1st cycle. Arguably, the inert MgO grains in the case of dolomite and ZrO_2 grains in the case of the composite would hinder aggregation of the nascent CaO crystals and their subsequent sintering. As the number of cycles evolves such steric hindrance effect would lose efficiency as these inert grains become progressively segregated from the CaO skeleton. In addition, aggregation and sintering would be enhanced at high pressure by compressive forces [37].

Note in Fig. 7d that the size of the MgO grains, which remain inert during the calcination/carbonation cycles, is increased under high pressure. This indicates that, regardless of the sintering mechanism associated to the $CaCO_3$/CaO transformation [32], sintering is also mechanically driven for dolomite at high temperature under a high pressure environment. In contrast, this effect is prevented by adding mechanically harder ZrO_2 to limestone (Figs. 7e-f). Thus, the composite shows a higher porosity than the natural carbonates and less segregation

of the inert grains, which would explain the better performance of the material under CaL–CSP conditions studied in our work.

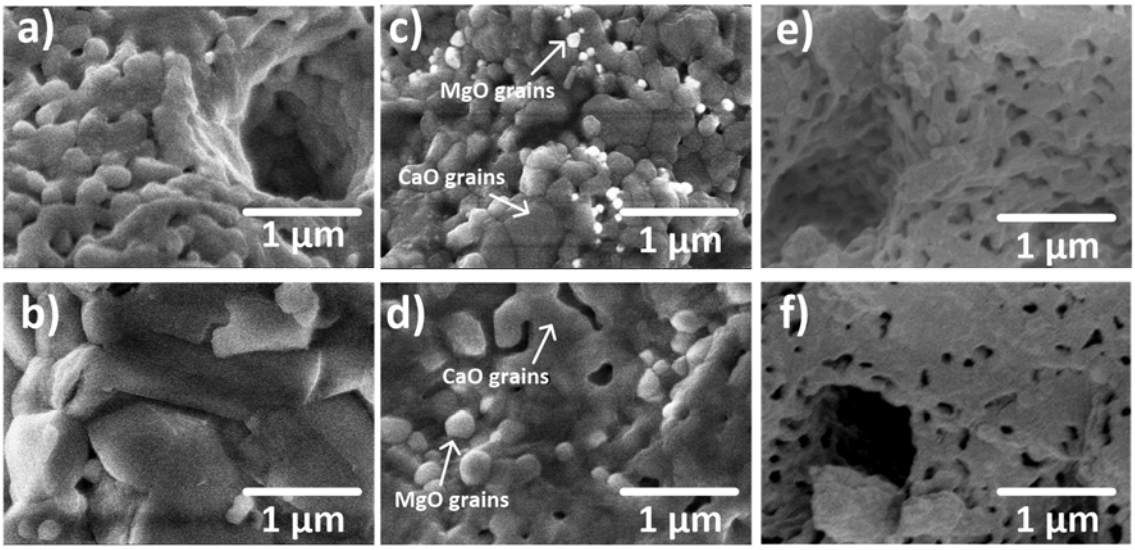

Fig. 7. SEM micrographs of the samples derived from natural limestone (a, b), dolomite (c, d) and the $ZrO_2/CaCO_3$ composite (e, f) after the CaL cycles for carbonation at absolute pressure of 1 bar (a, c, e) and under 3 bar of CO_2 (b, d, f).

Figure 8 illustrates the FIB-SEM tomography and compositional mappings obtained for the $ZrO_2/CaCO_3$ composite samples that result after the CaL cycles (ending in calcination) with carbonations at absolute pressure of 1 bar and under 3 bar of CO_2. As may be seen, the ZrO_2 grains remain homogeneously distributed in the solid structure in contrast with MgO grains in the case of dolomite, which segregate from the CaO skeleton. This homogeneous distribution of ZrO_2 in the CaO skeleton would prevent more effectively aggregation and sintering of the CaO grains.

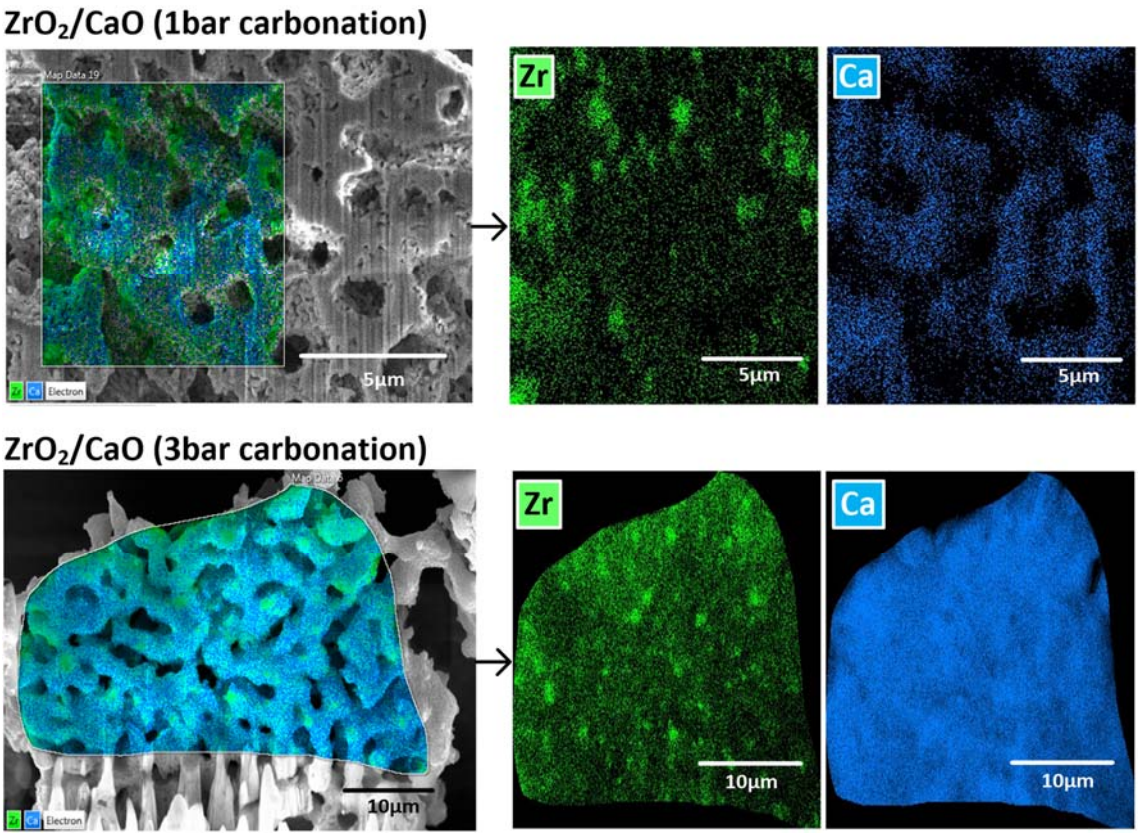

Fig. 8. FIB-SEM tomography and compositional mappings for the Zr and Ca elements of the $ZrO_2/CaCO_3$ composite sample after the CaL cycles (ending in calcination) under absolute pressure of 1 bar and 3 bar of CO_2.

Figure 9 shows SEM images of the CaO that results from the first calcination of limestone at 1000°C under absolute pressure of 1 bar of CO_2 and after calcination under absolute pressure of 1 bar of CO_2 with an increase of the pressure up to 3 bars just before decreasing the temperature for carbonation in the first cycle. As discussed above, increasing pressure at the end of the calcination stage is necessary in order to guarantee carbonation at high pressure. It may be seen in Fig. 9 that such increase of the reactor pressure at the end of the calcination stage, even for a short time period, promotes CaO sintering significantly, which would lead to a drop of conversion during the subsequent carbonation as observed in the first cycle (Fig. 4). As shown in previous studies, limestone derived CaO conversion scales proportionally to the CaO specific surface area available for carbonation ($X \propto S$) [30, 38]. Unfortunately, the sample mass used in our tests is not large enough to carry out a sufficiently robust physisorption analysis to obtain the CaO specific surface area. Nevertheless, a rough estimation may be inferred by approximating the CaO grains observed in the SEM images (Fig. 9) to smooth spheres of average diameter d [39], which gives a specific surface area $S \sim {}^{6}/_{\rho d}$, where $\rho = 3.37\ g/cm^3$ is the CaO solid density. The measured values of conversion in the first cycle for limestone derived CaO are $X_1(1\text{ bar}) \approx 0.43$ and $X_1(3\text{ bar}) \approx 0.25$, whereas the average CaO grain diameters (Fig. 9) are $d(1\text{ bar}) \approx 0.23$ µm and $d(3\text{ bar}) \approx 0.45$ µm. Thus, it is $X_1(1\text{ bar})/X_1(3\text{ bar}) \approx d(3\text{ bar})/d(1\text{ bar})$, which suggests that most of the hindering effect on carbonation takes place by enhanced CaO sintering at the end of the calcination stage when the reactor absolute pressure is increased just before carbonation.

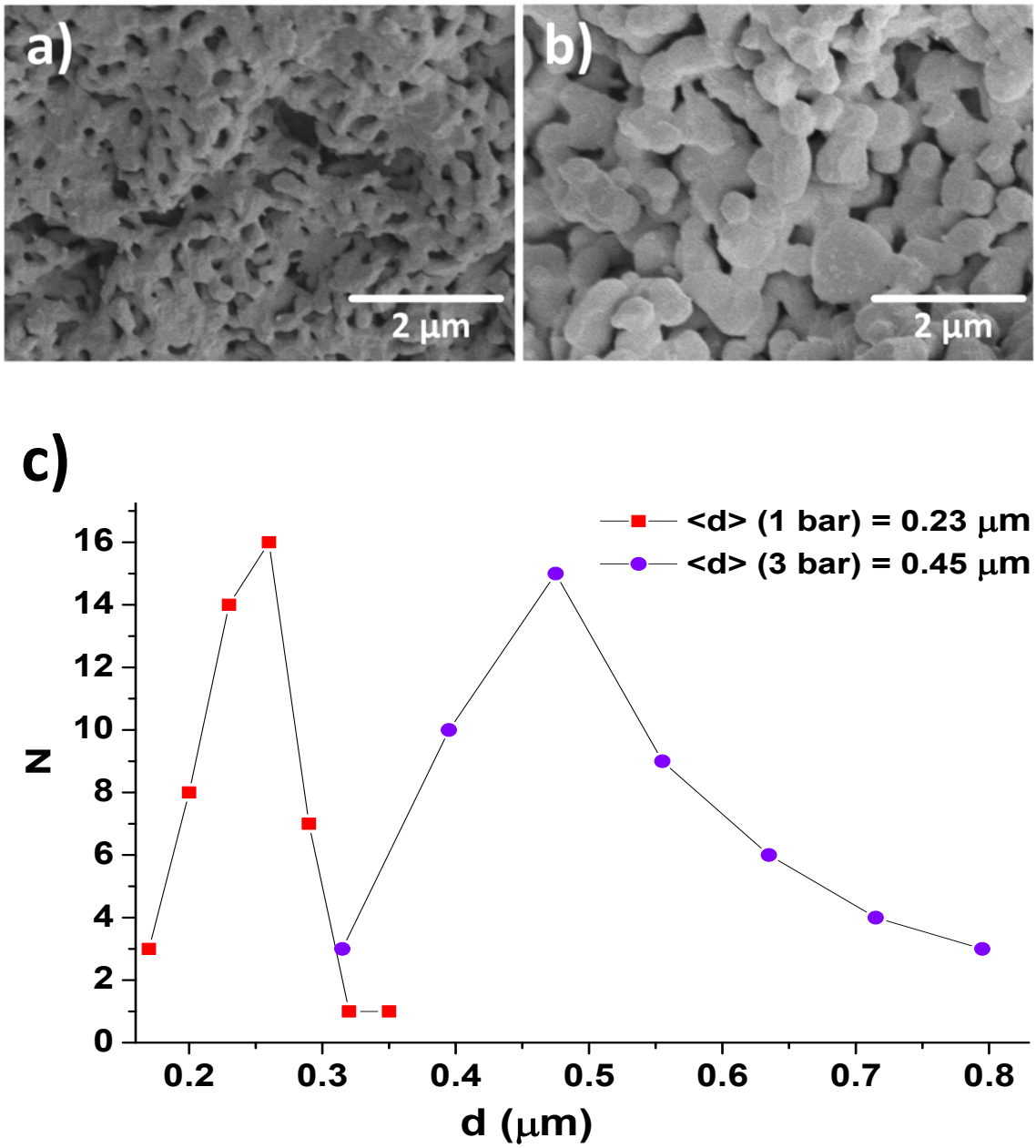

Fig. 9. Top: SEM micrographs of CaO derived from natural limestone after calcination at 1000°C under absolute pressure of 1 bar of CO_2 (a) and after calcination at 1000°C under absolute pressure of 1 bar of CO_2 ending with an increase of pressure up to 3 bars (b). Bottom: CaO grain size distributions measured from the SEM images (c) (the inset shows the average values).

Figure 10 shows SEM images of the samples after the CaL cycles (ending in carbonation). As can be observed, the carbonate layer built up in the carbonation stage is significantly sintered as would be expected since the Tamman temperature of $CaCO_3$ (around 500°C) is well below the carbonation temperature used in our experiments (850°C). Moreover, carbonation under high pressure leads to high compressive forces that would promote even further the sintering of the formed $CaCO_3$, as demonstrated for other materials [40]. In this case, an additional effect of the

marked $CaCO_3$ sintering is the notable segregation of the MgO grains in the dolomite sample (Fig. 10d), which arguably mitigates the thermal stabilizing role of MgO. In contrast, segregation in the $ZrO_2/CaCO_3$composite prepared by high energy milling is comparatively less marked as previously discussed. A further negative effect of the higher degree of $CaCO_3$ sintering under carbonation at high pressure (and therefore the increase of its crystallinity) is the progressive slowdown of decarbonation in the calcination stage (see Fig. 6, cycle 9th for limestone), which would require increasing the calcination temperature even above 1000°C for full calcination to be achieved. In the case of dolomite and the composite, the presence of inert grains would facilitate CO_2 desorption and decarbonation [41]. Accordingly, we observe that calcination takes place at a fast rate along all the cycles for dolomite and composite even in the case of high pressure tests.

A further relevant result obtained for the composite that may be inferred from the thermograms (N = 9 in Fig. 6) is that the slow carbonation phase (limited by solid-state diffusion) is significantly promoted. This diffusion controlled contribution to carbonation would be favored by the presence of Zr impurities evenly distributed in the CaO solid structure [42-43]. Thus, carbonation could be further enhanced by prolonging the solids residence time is the carbonator.

In our work we also tried to characterize the cycled samples by means of XRD and BET surface area analysis by N_2 sorption. The resulting coherent crystal length was beyond the maximum measurable (around 100 nm) and the surface area was about or below the measurement accuracy (around 1 m^2/g).

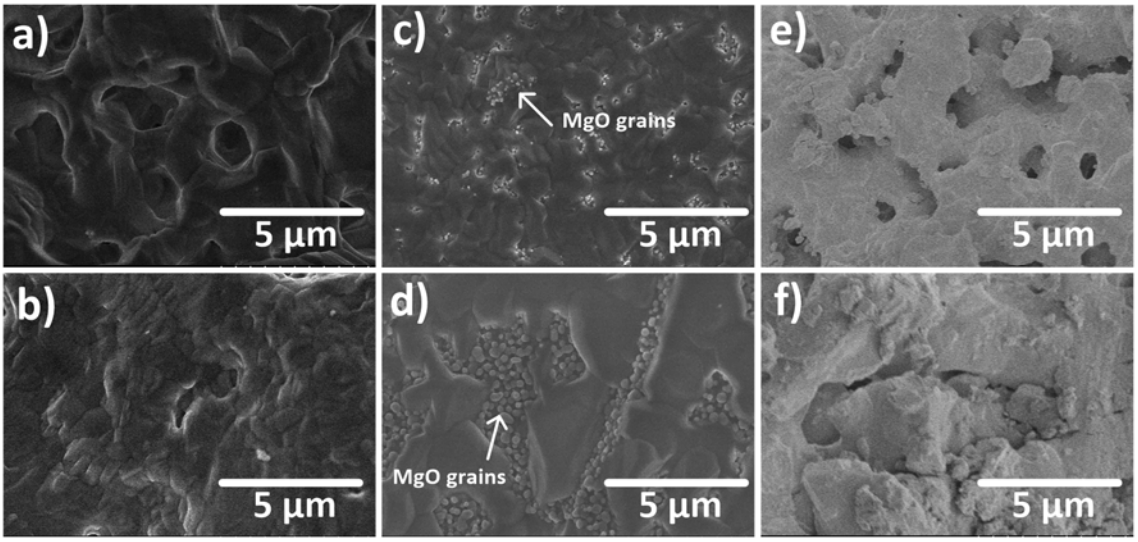

Fig. 10. SEM micrographs of samples after the CaL cycles (ending in carbonation) for natural limestone (a, b), dolomite (c, d) and $ZrO_2/CaCO_3$ composite (e, f). Carbonation under absolute pressure of 1 bar (a, c, e) and 3 bar (b, d, f).

CONCLUSIONS

This work analyzes the multicycle activity of natural carbonates (limestone and dolomite) and a composite (5 wt% ZrO_2 and 95 wt% natural limestone) prepared by high energy mechanical milling for their use in the Calcium-Looping process to store energy in Concentrated Solar Power

plants. The CaL-CSP integration studied in our work involves the cyclic calcination/carbonation of $CaCO_3$ under pure CO_2 at high temperature. According to the proposed scheme elsewhere, the excess CO_2 over the stoichiometric ratio effluent from the carbonator would be used by a gas turbine to generate electricity in a closed cycle. Thus, carbonation would be ideally carried out under high pressure to improve the thermoelectric conversion efficiency. If just one reactor is used for both reactions to reduce capital costs the absolute pressure of 1 bar must be increased up to the target high pressure for carbonation at the end of the calcination stage just before carbonation. Our thermogravimetric analysis results show that the multicycle CaO activity would be hindered in this short transient stage if the reactor pressure is increased just up to 3 bars. CaO sintering is notably promoted by the increase of pressure, which hampers the activity of the regenerated CaO. Moreover, the formed $CaCO_3$ during carbonation at high pressure is also notably sintered, which hinders decarbonation and CaO regeneration. Thus, the CaL multicycle performance of the samples analyzed is negatively affected by an increase of the reactor pressure. The presence of MgO inert grains in the case of dolomite is seen to mitigate CaO sintering, which reduces the loss of CaO reactivity and facilitates decarbonation. Nonetheless, an increase of the reactor pressure promotes a progressive MgO-CaO segregation mainly during the carbonation stage at high pressure and temperatures well over the $CaCO_3$ Tamman temperature, which hampers the enhanced performance of dolomite as the number of cycles is increased. The $ZrO_2/CaCO_3$ composite with a small mass percentage of inert solids (5 wt%) shows an enhanced conversion for both carbonation under absolute pressure of 1 bar and 3 bar. As inferred from the microscopy analysis, segregation of the inert grains is less marked in this composite as compared to dolomite, which would explain its superior performance. However, conversion drops at a similar rate with the number of cycles for both materials. Thus, the mechanism responsible for the progressive loss of conversion during cycling affects to a similar extent to both materials.

A detailed assessment on the implications for industrial scale deployment of our results is beyond the scope of our study. Nonetheless, we may use the values of conversion measured in the present work as affected by the reactor pressure to calculate the thermoelectric efficiency (η) according to the CaL-CSP integration model reported by our group elsewhere for limestone [18]. Thus, for a fixed pressure ratio PR=3 (ratio of carbonator pressure to turbine outlet pressure) and a value of conversion X=0.13, as measured in our work for limestone at N=11 when carbonation is carried out at 1 bar, would yield η=38%. The decrease of conversion down to X=0.06 when carbonation is carried out at 3 bars leads to a drop of efficiency by two percent points (η=36%). From the technical point of view, expanding to P=0.333 bar (when carbonation is carried out at 1 bar) would require a more complex design since heat exchangers, pipelines and other elements should work under low pressure. On the other hand, carrying out carbonation under atmospheric pressure would avoid the use of expensive lock-hoppers while the carbonator operation would be easier. A full techno-economic analysis remains to be carried out for an accurate evaluation of the conditions that maximize efficiency while technological complexity and costs are minimized. Taking into account the improvement of conversion observed in our work for dolomite and the $ZrO_2/CaCO_3$ composite compared to limestone it would be also useful to extend the integration model reported in [18] to the use of these materials.

Supporting Information

Elemental composition measured by X-Ray Fluerescence (XRF); Particle Size Distributions (PSDs) measured by means laser diffractometry; Calibration curve of the homemade thermobalance.

Acknowledgements

This work was supported by the Spanish Government Agency Ministerio de Economía y Competitividad (Contracts CTQ2014- 52763-C2 and CTQ2017-83602-C2, FEDER funds). The Microscopy service of the Innovation, Technology and Research Center of the University of Seville (CITIUS) is gratefully acknowledged and, in particular, the valuable help of Dr Francisco Varela. The authors also thank VPPI-US for the AP current contract.

References

1. Zhang, H. L.; Baeyens, J.; Degrève, J.; Cacères, G., Concentrated solar power plants: Review and design methodology. *Renewable and Sustainable Energy Reviews* **2013,** *22*, 466-481.
2. Fernández, A. G.; Ushak, S.; Galleguillos, H.; Pérez, F. J., Development of new molten salts with LiNO3 and Ca(NO3)2 for energy storage in CSP plants. *Applied Energy* **2014,** *119*, 131-140.
3. Sang, L.; Cai, M.; Zhao, Y.; Ren, N.; Wu, Y.; Burda, C., Mixed metal carbonates/hydroxides for concentrating solar power analyzed with DSC and XRD. *Solar Energy Materials and Solar Cells* **2015,** *140*, 167-173.
4. Wu, Y.-t.; Li, Y.; Ren, N.; Ma, C.-f., Improving the thermal properties of NaNO3-KNO3 for concentrating solar power by adding additives. *Solar Energy Materials and Solar Cells* **2017,** *160*, 263-268.
5. Barlev, D.; Vidu, R.; Stroeve, P., Innovation in concentrated solar power. *Solar Energy Materials and Solar Cells* **2011,** *95* (10), 2703-2725.
6. Kuravi, S.; Trahan, J.; Goswami, D. Y.; Rahman, M. M.; Stefanakos, E. K., Thermal energy storage technologies and systems for concentrating solar power plants. *Progress in Energy and Combustion Science* **2013,** *39* (4), 285-319.
7. Siva Reddy, V.; Kaushik, S. C.; Ranjan, K. R.; Tyagi, S. K., State-of-the-art of solar thermal power plants—A review. *Renewable and Sustainable Energy Reviews* **2013,** *27*, 258-273.
8. Jemmal, Y.; Zari, N.; Maaroufi, M., Thermophysical and chemical analysis of gneiss rock as low cost candidate material for thermal energy storage in concentrated solar power plants. *Solar Energy Materials and Solar Cells* **2016,** *157*, 377-382.
9. Pardo, P.; Deydier, A.; Anxionnaz-Minvielle, Z.; Rougé, S.; Cabassud, M.; Cognet, P., A review on high temperature thermochemical heat energy storage. *Renewable and Sustainable Energy Reviews* **2014,** *32*, 591-610.
10. Li, T. X.; Wu, S.; Yan, T.; Xu, J. X.; Wang, R. Z., A novel solid–gas thermochemical multilevel sorption thermal battery for cascaded solar thermal energy storage. *Applied Energy* **2016,** *161*, 1-10.
11. N'Tsoukpoe, K. E.; Liu, H.; Le Pierrès, N.; Luo, L., A review on long-term sorption solar energy storage. *Renewable and Sustainable Energy Reviews* **2009,** *13* (9), 2385-2396.
12. Mahlia, T. M. I.; Saktisahdan, T. J.; Jannifar, A.; Hasan, M. H.; Matseelar, H. S. C., A review of available methods and development on energy storage; technology update. *Renewable and Sustainable Energy Reviews* **2014,** *33*, 532-545.
13. Edwards, S. E. B.; Materic, V., Calcium looping in solar power generation plants. *Solar Energy* **2012,** *86* (9), 2494-2503.

14. Sakellariou, K. G.; Karagiannakis, G.; Criado, Y. A.; Konstandopoulos, A. G., Calcium oxide based materials for thermochemical heat storage in concentrated solar power plants. *Solar Energy* **2015,** *122*, 215-230.
15. Barker, R., REVERSIBILITY OF REACTION CACO3 REVERSIBLE CAO+CO2. *Journal of Applied Chemistry and Biotechnology* **1973,** *23* (10), 733-742.
16. Barker, R., The reactivity of calcium oxide towards carbon dioxide and its use for energy storage. *Journal of Applied Chemistry and Biotechnology* **1974,** *24* (4-5), 221-227.
17. Flamant, G.; Hernandez, D.; Bonet, C.; Traverse, J.-P., Experimental aspects of the thermochemical conversion of solar energy; Decarbonation of CaCO3. *Solar Energy* **1980,** *24* (4), 385-395.
18. Chacartegui, R.; Alovisio, A.; Ortiz, C.; Valverde, J. M.; Verda, V.; Becerra, J. A., Thermochemical energy storage of concentrated solar power by integration of the calcium looping process and a CO2 power cycle. *Applied Energy* **2016,** *173*, 589-605.
19. Cot-Gores, J.; Castell, A.; Cabeza, L. F., Thermochemical energy storage and conversion: A-state-of-the-art review of the experimental research under practical conditions. *Renewable and Sustainable Energy Reviews* **2012,** *16* (7), 5207-5224.
20. R. Chacartegui, e. a. Sistema de almacenamiento de energía termoquímica a partir fuente térmica a media temperatura basado en la integración de ciclo calcinacióncarbonatación (Calcium Looping) y ciclo cerrado de potencia de CO2. Patent. P201500493.
21. Ortega-Fernández, I.; Calvet, N.; Gil, A.; Rodríguez-Aseguinolaza, J.; Faik, A.; D'Aguanno, B., Thermophysical characterization of a by-product from the steel industry to be used as a sustainable and low-cost thermal energy storage material. *Energy* **2015,** *89*, 601-609.
22. Blamey, J.; Anthony, E. J.; Wang, J.; Fennell, P. S., The calcium looping cycle for large-scale CO2 capture. *Progress in Energy and Combustion Science* **2010,** *36* (2), 260-279.
23. Ball, R., Using the second law first: Improving the thermodynamic efficiency of carbon dioxide separation from gas streams in an Endex calcium looping system. *Applied Thermal Engineering* **2015,** *74* (Supplement C), 194-201.
24. Kierzkowska, A. M.; Pacciani, R.; Mueller, C. R., CaO-Based CO2 Sorbents: From Fundamentals to the Development of New, Highly Effective Materials. *Chemsuschem* **2013,** *6* (7), 1130-1148.
25. Garcia-Labiano, F.; Abad, A.; de Diego, L. F.; Gayan, P.; Adanez, J., Calcination of calcium-based sorbents at pressure in a broad range of CO2 concentrations. *Chem. Eng. Sci.* **2002,** *57* (13), 2381-2393.
26. Baker, E. H., 87. The calcium oxide-carbon dioxide system in the pressure range 1-300 atmospheres. *Journal of the Chemical Society (Resumed)* **1962,** (0), 464-470.
27. Kyaw, K.; Kubota, M.; Watanabe, F.; Matsuda, H.; Hasatani, M., Study of Carbonation of CaO for High Temperature Thermal Energy Storage. *JOURNAL OF CHEMICAL ENGINEERING OF JAPAN* **1998,** *31* (2), 281-284.
28. Butler, J. W.; Lim, C. J.; Grace, J. R., CO2 capture capacity of CaO in long series of pressure swing sorption cycles. *Chemical Engineering Research and Design* **2011,** *89* (9), 1794-1804.
29. Yates, J. G., Lettieri, Paola. , *Fluidized-Bed Reactors: Processes and Operating Conditions*. Springer, 2016.
30. Valverde, J. M., A model on the CaO multicyclic conversion in the Ca-looping process. *Chemical Engineering Journal* **2013,** *228*, 1195-1206.
31. Sun, Z.; Luo, S.; Qi, P.; Fan, L.-S., Ionic diffusion through Calcite (CaCO3) layer during the reaction of CaO and CO2. *Chem. Eng. Sci.* **2012,** *81*, 164-168.
32. Alovisio, A.; Chacartegui, R.; Ortiz, C.; Valverde, J. M.; Verda, V., Optimizing the CSP-Calcium Looping integration for Thermochemical Energy Storage. *Energy Conversion and Management* **2017,** *136*, 85-98.

33. Larker, H. T., RECENT ADVANCES IN HOT ISOSTATIC PRESSING PROCESSES FOR HIGH-PERFORMANCE CERAMICS. *Materials Science and Engineering* **1985,** *71* (1-2), 329-332.
34. Valverde, J. M.; Sanchez-Jimenez, P. E.; Perez-Maqueda, L. A., Relevant Influence of Limestone Crystallinity on CO2 Capture in The Ca-Looping Technology at Realistic Calcination Conditions. *Environmental Science & Technology* **2014,** *48* (16), 9882-9889.
35. Perejón, A.; Romeo, L. M.; Lara, Y.; Lisbona, P.; Martínez, A.; Valverde, J. M., The Calcium-Looping technology for CO2 capture: On the important roles of energy integration and sorbent behavior. *Applied Energy* **2016,** *162*, 787-807.
36. Sánchez-Jiménez, P. E.; Valverde, J. M.; Perejón, A.; de la Calle, A.; Medina, S.; Pérez-Maqueda, L. A., Influence of Ball Milling on CaO Crystal Growth During Limestone and Dolomite Calcination: Effect on CO2 Capture at Calcium Looping Conditions. *Crystal Growth & Design* **2016,** *16* (12), 7025-7036.
37. Butler, J. W.; Lim, C. J.; Grace, J. R., CO2 capture capacity of CaO in long series of pressure swing sorption cycles. *Chemical Engineering Research & Design* **2011,** *89* (9), 1794-1804.
38. Grasa, G. S.; Abanades, J. C., CO2 Capture Capacity of CaO in Long Series of Carbonation/Calcination Cycles. *Industrial & Engineering Chemistry Research* **2006,** *45* (26), 8846-8851.
39. Borgwardt, R. H., Calcium oxide sintering in atmospheres containing water and carbon dioxide. *Industrial & Engineering Chemistry Research* **1989,** *28* (4), 493-500.
40. German, R. M., *Sintering theory and practice*.
41. de la Calle Martos, A.; Valverde, J. M.; Sanchez-Jimenez, P. E.; Perejon, A.; Garcia-Garrido, C.; Perez-Maqueda, L. A., Effect of dolomite decomposition under CO2 on its multicycle CO2 capture behaviour under calcium looping conditions. *Physical Chemistry Chemical Physics* **2016,** *18* (24), 16325-16336.
42. Anderson, T. F., Self-diffusion of carbon and oxygen in calcite by isotope exchange with carbon dioxide. *Journal of Geophysical Research* **1969,** *74* (15), 3918-3932.
43. Anderson, T. F., Self-diffusion of carbon and oxygen in dolomite. *Journal of Geophysical Research* **1972,** *77* (5), 857-861.

For Table of Contents Use Only

Dolomite and $ZrO_2/CaCO_3$ exhibit a significantly improved multicycle performance under high pressure compared to limestone for energy storage of Concentrated Solar Power.